DOI: http://doi.org/10.15446/ing.investig.119286

Research article/Mechanical Engineering, Mechatronics, and Materials Science

Investigating the Mechanical, Wear, and Thermal Attributes of Aluminum Zirconium Nanocomposite Synthesis through the Powder Metallurgy Process

Investigación de los atributos mecánicos, de desgaste y térmicos de la síntesis de nanocompuestos de aluminio y circonio mediante el proceso de metalurgia en polvo

Kalaimani Maniarasu*[1] and Shaafi Tajdueen[2]

ABSTRACT

This article reports the results of a study that examined the wear and thermal behavior of Al/ZrO_2 nanocomposites fabricated using powder metallurgy with different ZrO_2 reinforcement contents (3, 6, and 9 wt.%). The findings show that microhardness increased to 33 HV in sample AZ0, 58 HV in AZ3, 74 HV in AZ6, and 87 HV in AZ9, indicating that higher ZrO_2 content leads to enhanced surface resistance. The tensile strength of sample AZ0 was 285 MPa, with elongation values decreasing to 6%, which demonstrates a transition from more ductile performance to increased mechanical strength with the addition of reinforcement material. Compressive strength also exhibited a significant improvement, increasing from 43 MPa in AZO to 376 MPa in AZ9, indicating enhanced load-bearing capacity in the reinforced composite. The coefficient of friction decreased markedly from 1.6 to 0.4, reflecting improved wear resistance due to the homogeneous distribution of ZrO_2 nanoparticles and the formation of a hard ceramic phase. Thermal conductivity also decreased from 237 $Wm^{-1}K^{-1}$ to 150 $Wm^{-1}K^{-1}$, which is attributed to the low thermal conductivity of ZrO_2 and its homogeneous incorporation into the matrix. Similarly, the coefficient of linear thermal expansion decreased from $22x10^{-6}$/K to $11x10^{-6}$/K, owing to the thermal barrier effect and dimensional stability provided by the ceramic reinforcement. Overall, these results demonstrate that ZrO_2 nanoparticles have the potential to enhance the mechanical strength, wear resistance, and thermal stability of aluminum nanocomposites.

Keywords: sintering process, zirconium dioxide, wear coefficient of friction, coefficient of linear thermal expansion

RESUMEN

Este artículo reporta los resultados de un estudio que examinó el desgaste y el comportamiento térmico de nanocompuestos de Al/ZrO_2 fabricados mediante metalurgia de polvos con diferentes refuerzos de ZrO_2 (3, 6 y 9 % en peso). Los resultados muestran que la microdureza aumentó a 33 HV en AZ0, a 58 HV en AZ3, a 74 HV en AZ6 y a 87 HV en AZ9, indicando que un mayor contenido de ZrO_2 aumenta la resistencia de la superficie del material. La resistencia a la tracción de la muestra AZ0 fue de 285 MPa, y su elongación alcanzó hasta el 6 %, lo que evidencia una transición desde un comportamiento más dúctil hacia uno de mayor resistencia mecánica con la adición del refuerzo. La resistencia a la compresión también evidenció una mejora significativa, con un aumento a 43 MPa en AZ0 y a 376 MPa en AZ9, lo que indica una mayor capacidad de carga del compuesto reforzado. El coeficiente de fricción se redujo considerablemente (de 1.6 a 0.4), indicando un aumento de la resistencia al desgaste debido a la distribución homogénea de las nanopartículas de ZrO_2 y la formación de una fase cerámica dura. La conductividad térmica se redujo de 237 $Wm^{-1}K^{-1}$ a 150 $Wm^{-1}K^{-1}$, lo cual se debe a la baja conductividad térmica del ZrO_2 y su incorporación homogénea en la matriz. De manera similar, el coeficiente de expansión térmica lineal disminuyó de $22x10^{-6}$/K a $11x10^{-6}$/K, lo cual se explica por el efecto de barrera térmica y la estabilidad dimensional proporcionada por el refuerzo cerámico. En general, estos resultados demuestran que las nanopartículas de ZrO_2 tienen el potencial de mejorar la resistencia mecánica, la resistencia al desgaste y la estabilidad térmica de los nanocompuestos de aluminio.

Palabras clave: proceso de sinterización, dióxido de circonio, coeficiente de fricción por desgaste, coeficiente de expansión térmica lineal

Received: March 10 2025
Accepted: December 15 2025

[1]Department of Mechanical Engineering, Prathyusha Engineering College, Thiruvallur, Tamil Nadu India. Email: mkalaikvn@gmail.com
[2]Department of Mechanical Engineering, Saveetha School of Engineering, Saveetha Institute of Medical and Technical Sciences (SIMATS), Chennai, India. Email: shaafit.sse@saveetha.com

Graphical abstract

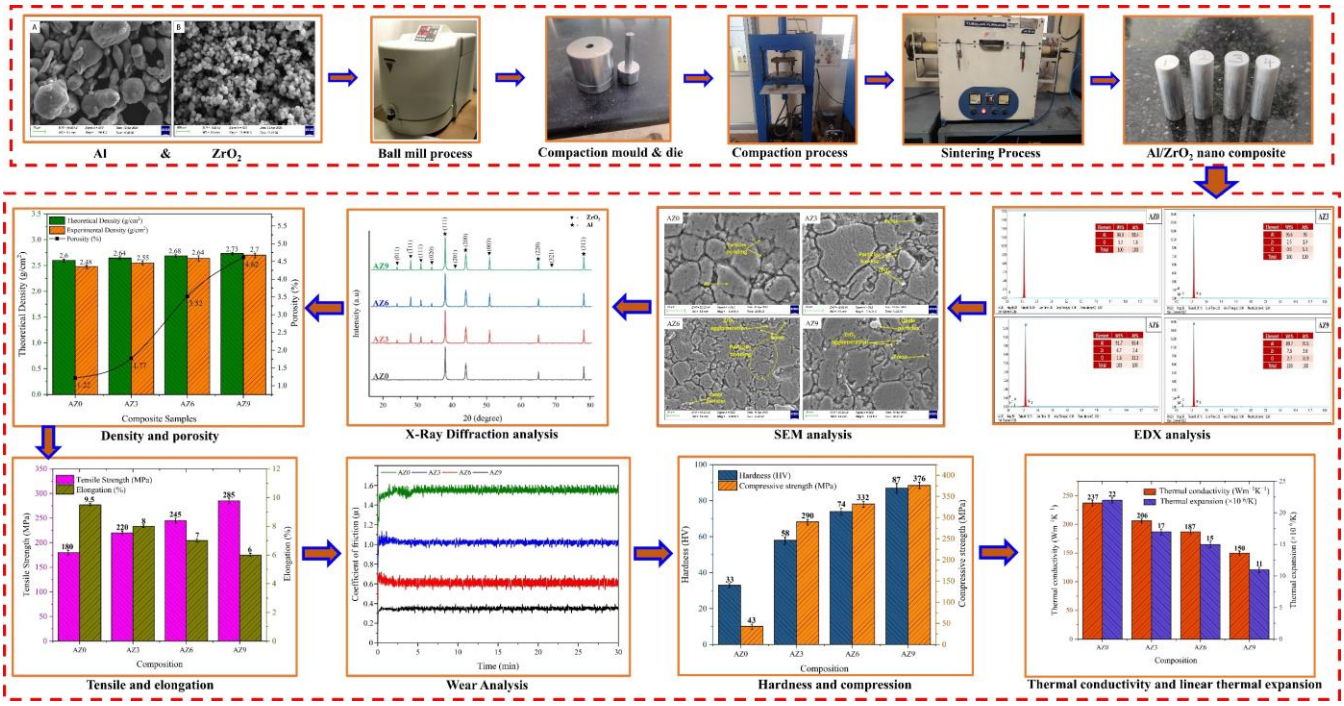

Introduction

Advanced composite materials have been extensively investigated for high-performance applications in the aerospace and automotive industries. Current research focuses on achieving high strength-to-weight ratios for enhancing mechanical, wear, and thermal stability. These types of materials are designed to enhance performance under diverse environmental conditions. Improvements in composite material properties are achieved through the incorporation of ceramic reinforcement particles at varying weight percentages. Typical ceramic reinforcements include SiC, TiC, SiO_2, B_4C, Si_3N_4, TiO_2, Al_2O_3, and ZrO_2. Among these, zirconia (zirconium dioxide, or ZrO_2) is one of the most extensively researched engineering ceramic materials due to its notable properties, which include excellent mechanical qualities, chemical inertness, thermal stability, and a wide band gap [1]. Depending on its crystal structure, the density of zirconia ranges from 5.68 to 6.08 g/m³. It exhibits high hardness (≈1200 HV), a bending strength in the range of 900-1200 MPa, and a compressive strength of 2000 MPa relative to that of steel. However, its fracture toughness is relatively low (7-10 MPa/m²), despite maintaining a Young's modulus of approximately 210 GPa and a coefficient of thermal expansion of 11 x 10^{-6}/K. Nevertheless, through stabilization, its fracture resistance can be significantly improved. ZrO_2 exists in three polymorphs of ZrO_2 that depend on temperature: monoclinic (m-ZrO_2), stable below 1150 °C; tetragonal (t-ZrO_2), stable between 1150 and 2370 °C; and cubic (c-ZrO_2), stable above 2370 °C [2],[3]. The grain structure and the resulting material properties of zirconia are strongly influenced by the concentration of Y_2O_3. Yttria-stabilized zirconia (3 mol.% Y_2O_3) has been widely applied as a bone substitute and an oxygen transport membrane due to its enhanced fracture toughness and pore structure [4]. Doping ZrO_2 with rare-earth elements remains an emerging field of study, which has already led to the discovery of new applications for these materials, given their remarkable properties, including stability at elevated temperatures, low thermal conductivity, high melting points, and resistance to molten salt corrosion [5].

Aluminum matrix composites with nanoscale reinforcement enable the precise control of material behavior at the molecular and grain-structure levels. This approach allows for the effective tailoring of microstructures and properties through nanoscale design and fabrication, resulting in functional systems with improved mechanical properties, wear resistance, and low thermal expansion [6]. Aluminum nanocomposites synthesized via powder metallurgy exhibit low porosity ranged from 2 % [7]. Several studies have reported improvements in the mechanical and wear characteristics of aluminum nanocomposites fabricated via metallurgy, as this method has proven to be an effective approach for enhancing the performance of MMC products. The production of alumina-zirconia composites through powder metallurgy involves using ZrO_2 contents at three different ratios (from 5 to 15 %). These materials are evaluated in terms of hardness, wear rate, electrical resistance, and thermal expansion behavior. SEM analysis has revealed a uniform distribution of ZrO_2 particles, which limits agglomeration, leading to enhanced mechanical and electrical properties [8]. Another research work explored Al 2024 composites reinforced with 5-20 wt.% ZrO_2 nanoparticles fabricated through vacuum infiltration. The incorporation of ZrO_2 increased particle density, strength, and wear resistance, although it compromised the cross-breaking properties. These findings confirm the effectiveness of ZrO_2 in enhancing the mechanical characteristics of Al 2024 alloys [9], [10]. Similarly, AA6063/ZrO_2 metal matrix composites fabricated via stir casting with ZrO_2 additions of 0, 2, and 4 wt.% demonstrated significant improvements in hardness, tensile strength, and wear resistance. Tensile tests revealed that ZrO_2 composites containing 4 wt.% ZrO_2 achieve a maximum hardness of 71.0 HV, an ultimate tensile strength of 168.384 MPa, and the lowest wear rate among the investigated samples. SEM analysis confirmed

a uniform distribution of ZrO_2 particles, which enhanced the mechanical qualifying features of the composite structure [11].

Aluminum matrix composites can be fabricated using various processing routes, including liquid-state, solid-state, and two-state alternatives. Among these, solid-state powder metallurgy offers distinct advantages over the liquid- and two-phase processes. Common challenges in composite fabrication, such as the uneven distribution of reinforcement particles, porosity, and bonding strength and hardness, are effectively mitigated through powder metallurgy. This technique enables a fine microstructural control, is particularly more suitable for handling nano-reinforcement particles, and operates at relatively low processing temperatures. Consequently, powder metallurgy is the best strategy that can be used to produce a high-quality aluminum nanocomposite that is both reliable and efficient. Aluminum hybrid nanocomposites reinforced with SiC and various ZrO_2 concentrations have been successfully fabricated using spark plasma sintering. Scanning electron microscopy (SEM) analyses have revealed a balanced distribution, while mechanical testing has demonstrated that the addition of ZrO_2 significantly improves wear resistant and damage tolerance. According to a recent study, a specimen with an Al/5 % SiC/15 % ZrO_2 composition (S4) exhibited the highest hardness and wear resistance among all evaluated samples [12]. Similarly, Ti6Al4V composites reinforced with ZrO_2 were fabricated using a powder metallurgical process and evaluated through mechanical testing and microstructure analysis. Compressive strength, hardness, and thermal expansion properties improved with increasing ZrO_2 contents. The composite containing 6 wt.% ZrO_2 achieved the best overall properties, making it suitable for aviation and automotive applications [13].

Welding is a solid-state joining technique that offers significant advantages in terms of mechanical performance and weld quality, and it is commonly friction stirred. For instance, the incorporation of TiCnp into AZ31 Mg alloys resulted in a tensile strength of 230 MPa, a micro-hardness of 70 MPa, an impact strength of 89.34 MPa, a wear rate of 0.0046 m^3/m, and a peak tensile strength of 242 MPa. Welds are enhanced to reinforce mechanical properties with the right concentration of TiCnp [14], [15].

[16] investigated the structure and physical characteristics of Al/SiC/ hybrid composites fabricated through the Spark Plasma Sintering (SPS) process. Their results showed that ZrO_2 additions enhances densification, hardness, and compressive strength while only causing minimal reductions in elongation. The best overall mechanical performance was observed in the S4 specimen (Al/5 % SiC/15 % ZrO_2). [17] reported that a newly developed barrel mixer reduces mixing duration in half compared to V-blenders, while achieving higher performance when mixing Al-MMC powders. Additionally, the use of cyanoamides improved SiC reinforcement uniformity, which resulted in increases of 10-20% in hardness and 8-20% in compression strength. [18] investigated Al6061 alloy composites containing ZrO_2 nanoparticles (0-6 wt.%), which were produced through stir casting. Their study evaluated physical and mechanical behavior, as well as the tribological properties of the composites. The tribological analysis indicated that increasing the ZrO_2 nanoparticle content resulted in enhanced hardness and tensile strength, improved wear resistance, and reduced elongation. The researchers attributed these improved properties to the microstructural features observed in SEM analyses of fracture surfaces and wear areas, which warrant further research.

This study sought to prepare aluminum nanocomposites using the powder metallurgy technique. Key stages of this process included the preparation of the base matrix, the selection of reinforcement ratios, powder blending, and compaction. During the sintering phase, temperature was slowly raised with the supply of argon gas, which was meant to react with oxide reinforcements, eliminating gas and air pores from the samples. This step was critical, as it enhanced particle bonding strength, promoted densification, and decreased nanoparticles agglomeration.

The overall objective of our work was to improve the microhardness, tensile strength, compressive strength, and wear behavior, including the friction coefficient of aluminum through the uniform distribution of ceramic (ZrO_2) nanoparticles. Variations in thermal conductivity and thermal expansion were also investigated, with ZrO_2 acting as thermal barrier in the matrix. Accordingly, this work aimed to develop lightweight, high-performance composite materials suitable for structurally and thermally demanding applications in the aerospace, automotive, and defense industries.

Materials methods

Details of the matrix and reinforcing materials

The powder metallurgy process was used to fabricate nanocomposites with varying ZrO_2 reinforcement contents, with pure aluminum serving as the base matrix. Aluminum powders with particle sizes ranging from 30 to 50 µm and ZrO_2 nanoparticles with sizes between 30 and 50 nm were procured from Vedayukt India Pvt. Ltd. (Jharkhand, India).

Figure 1 presents the SEM images, particle size distribution, and EDX spectra of the studied (a) aluminum (Al) microparticles and (b) ZrO_2 nanoparticles. The SEM image of the Al microparticles reveals large and irregularly shaped particles. The corresponding EDX spectrum indicates that the sample is mostly composed of Al, with a weight percentage of 98.8% and an atomic percentage of 98.4%, *i.e.*, it is predominantly made of pure aluminum. A minor oxygen (O) peak, corresponding to 1.2 wt.% and 1.6 at.%, is also observed, indicating a thin oxide coating on the surface, a common characteristic of air exposed aluminum. Conversely, the SEM image of the ZrO_2 nanoparticles shows significantly smaller, spherical particles. The EDX spectrum reveals zirconium (Zr) contents of 65.31 wt.% and 24.82 at.%, while the oxygen level accounts for 34.69 wt.% and 75.18 at.%, confirming the presence of typical ZrO_2 nanoparticles. These findings demonstrate the purity and surface properties of the two different particles, indicating low oxidation levels in the Al microparticles and a high oxidation in the Zr oxide nanoparticles. These characteristics are relevant to the application of ZrO_2 in catalysis, ceramics, and biomaterials. The EDX spectra are detailed and provide a clear picture of the elemental composition of the studied material.

Experimental method

Figure 2 shows the fabrication of Al/ZrO_2 nanocomposites with varying reinforcement proportions using powder metallurgy. The nanocomposite samples were produced with the help of a high-speed steel cylindrical mold and die with dimensions of 10 mm in diameter and 50 mm in length. The green compacted samples were then sintered in a tubular furnace. Mechanical characterizations of the sintered nanocomposite samples included density, microhardness, compressive strength, elongation, and tensile strength. Wear resistance was evaluated using a pin-on-disc apparatus, while thermal properties were assessed with a dilatometer.

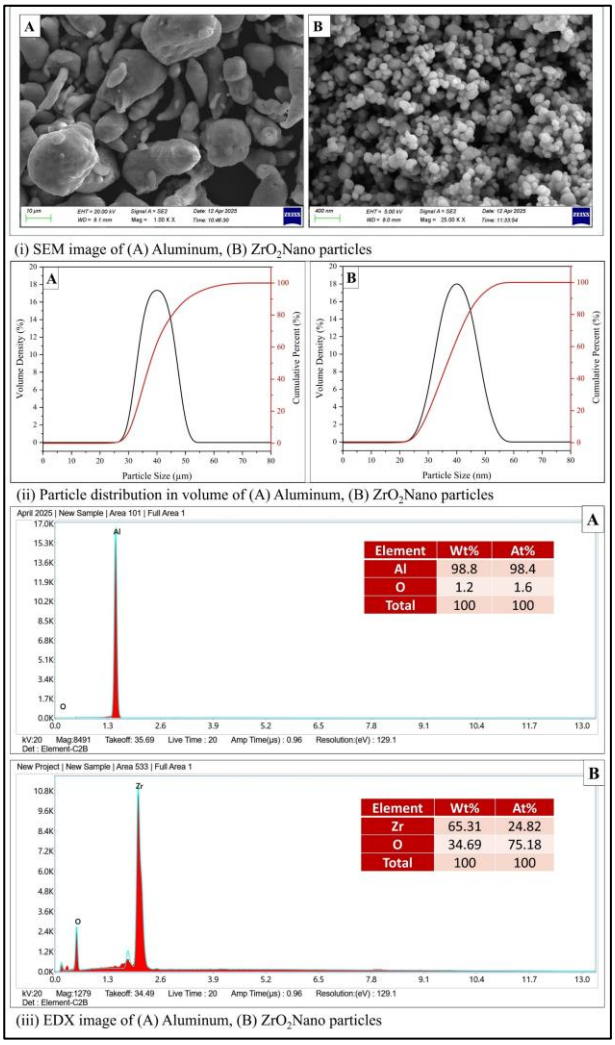

Figure 1. (i) SEM, (ii) particle size, and (iii) EDX analysis of Al and ZrO_2 nanoparticles
Source: Authors

Table I. Sample names and composition

No.	Name	Composition
1	AZ0	Al
2	AZ3	Al/3%ZrO_2
3	AZ6	Al/6%ZrO_2
4	AZ9	Al/9%ZrO_2

The AZ0, AZ3, AZ6, and AZ9 samples were fabricated with the designated weight percentage of the reinforcing particles, as shown in Table and Figure 3. The powder metallurgy process employed for the fabrication of aluminum nanocomposite is illustrated in Figure 3. Stearic acid was used as a lubricant in amounts ranging from 0.5 to 1.5% by mass of powder for each composition, and it was mixed at room temperature for 1 h at 150 rpm using a planetary ball mill (Figure 3). To ensure a homogeneous distribution of the ceramic particles within the aluminum matrix, five tungsten carbide balls with a diameter of 5 mm were employed during milling. After mixing, the powder blend was transferred into a high-speed steel mold and die (Figure 3). Cold compaction was performed at a pressure of 600 MPa, in order to produce cylindrical green compacts measuring 10 mm in diameter and 50 mm in length (Figure 3). The compacts were arranged in the ceramic cup and inserted into the tubular furnace (Figure 3) under an argon atmosphere to avoid oxidation and reduce thermal stress. Prior to sintering, argon gas was introduced and maintained at a 2 L/min flow rate (Figure 3). The furnace temperature was raised at a rate of 5 °C/min until a value of 550 °C was reached, while the continuous argon flow was maintained to inhibit aluminum oxidation. The material remained at 550 °C for 1 h to promote particle bonding. Al oxidation at elevated temperatures was mitigated by the argon atmosphere, which removed oxygen. Sintering was followed by a slow cooling of the furnace. Argon was still allowed to flow through the furnace to minimize the thermal stress caused by extreme fluctuations in temperature—a rapid cooling of the material would result in the creation of thermal gradients, generating internal stresses that could compromise the integrity of the composite. The temperature was allowed to decrease to below 300 °C, and then the flow of argon was slowly halted. We used a controlled sintering environment, ensuring low oxidation and thermal stress, as well as the quality of the nanocomposites in Figure 3.

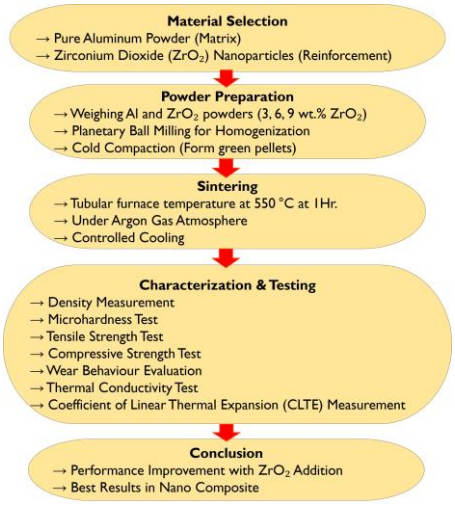

Figure 2. Flow diagram of our research methodology
Source: Authors

Nanocomposites characterization

Theoretical and experimental density

The Archimedes principle was used to determine the experimental density (ρ_{Exp}) of each nanocomposite. Using a digital scale, an ASTM D 792-66 experiment was carried out, wherein the weight was measured against the expected value. The testing procedure involved determining the nanocomposite sample AZ9 mass of 150 g on a digital weighing scale. The nanocomposite sample volume was measured by filling a glass vessel with water to determine its mass. An initial measurement of 300 ml was recorded. The nanocomposite samples were placed into the glass vessel, and the final water level was recorded at 354 ml. The total number of nanocomposite samples in AZ9 was determined by measuring the increase in the water level to 354 ml from the initial 300 ml. The resulting water difference was 54 ml. The volume and weight principles were calculated using Eq. (1) [19]. The nanocomposite sample density in AZ9 was determined to be 2.76 g/cm³.

$$Experimental\ density(\rho_{Exp}) = \left(\frac{Mass(g)}{Volume(cm^3)}\right) \quad (1)$$

The calculation of the theoretical density (ρ_{Th}) of the Al/ZrO_2 nanocomposite depended on the mass fractions of pure aluminum

Figure 3. Fabrication of Al/ZrO_2 nanocomposites: a) Al and ZrO_2 particle, b) ball mill process, c) mold and die, d) compaction process, e) sintering process, f) Al/ZrO_2 nanocomposites, g) temperature and argon flow during sintering
Source: Authors

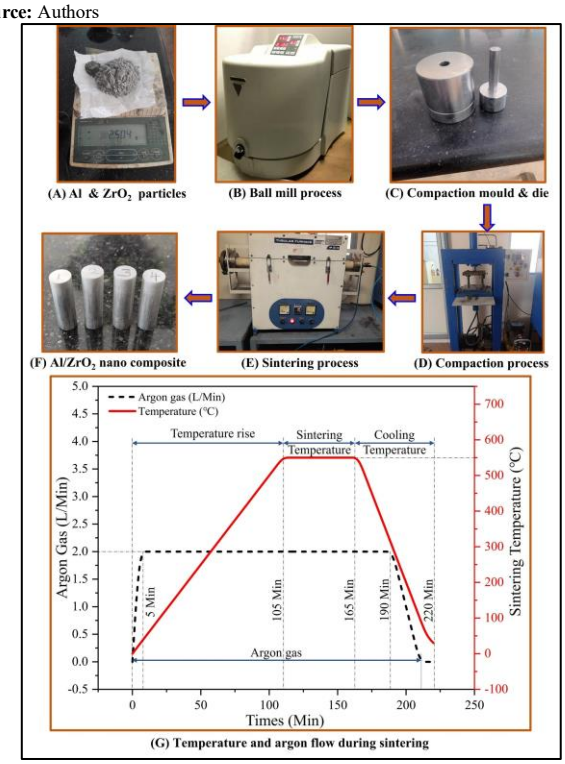

(m_{Al}) and zirconium dioxide (m_{ZrO_2}). The density values for aluminum (ρ_{Al}=2.6 g/cm³) and zirconium dioxide (ρ_{ZrO_2}=5.68 g/cm³) were utilized in calculating the rule of mixtures, as shown in Eq. (2) [20].

$$Theoretical\ density(\rho_{Th}) = \left(m_{Al}.\rho_{Al} + m_{ZrO_2}.\rho_{ZrO_2}\right) \quad (2)$$

The porosity of the samples was determined using the Archimedes method, as outlined in Eq. (3) [21].

$$Porosity\,(\%) = \left(\frac{\rho_{Th} - \rho_{Exp}}{\rho_{Th}}\right) \times 100 \quad (3)$$

where, ρ_{Th} is the theoretical density (g/cm³) and ρ_{Exp} is the experimental density (g/cm³).

Density of green compaction and sintered nanocomposites

The Al nanocomposite samples were prepared by blending powders with different reinforcement contents, as listed in Table . A hydraulic press was used to compress the samples at a constant pressure of 600 MPa, with a holding time of 10 min. Sintering was carried out for 1 h at a temperature of 550 °C. The compaction densities were measured immediately after the compaction process. These values were subsequently compared with experimental densities in order to determine their densification behavior. The findings indicated that the green compaction density increased when ZrO_2 was added—the densities of AZ0 and AZ9 were 2.36 and 2.63 g/cm³, respectively. This trend suggests that the increasing the ZrO_2 reinforcement content enhances the overall density of the material, which is generally associated with improved mechanical performance and material properties. A similar trend was observed in the experimental densities after sintering, with the AZ9 sample exhibiting the highest density (2.7 g/cm³). The density of the green sample compaction and the sintered samples varied the most when the percentage of ZrO_2 was higher, with the best differences observed for AZ6 and AZ9. This behavior indicates that the sintering process was successful in minimizing porosity and enhancing the cohesion of the material, especially in the composite with stronger reinforcement. The findings reveal that the addition of ZrO_2 promotes the densification of the aluminum matrix, with AZ9 producing the most favorable results in terms of green compaction and sintered density. This outcome demonstrates the positive impact of ZrO_2 strengthening on the overall characteristics of the material.

Microhardness

A microhardness test was performed using a Shimadzu HMV-2 Vickers tester in accordance with ASTM E384, at a temperature of 25 °C. The test consisted of applying a standard indenter with a defined geometry on the surface of the test material, with a load of 500 gf (4.90 N), for a period of 10 s. The diagonal lengths of the depressions (d_1 and d_2) were optically measured for each sample based on three indentation tests. The microhardness value was determined using Eqs. (4) and (5) [22], where HVN denotes the Vickers hardness number, d is the median diagonal length (mm), and F is the load (gf).

$$HVN = \left(1854.4 \times \frac{F}{d^2}\right) \quad (4)$$

$$d = \left(\frac{d_1 + d_2}{2}\right) \quad (5)$$

Tensile and compressive strength

Tensile and compressive tests were conducted using a computer-assisted hydraulic universal tensile testing machine (UTM) in accordance with ASTM E-8-04 [23], at a room temperature of 30 °C. The gauge length of the specimen was set at 25 mm, while a crosshead speed of 2.5 mm/min was consistently maintained. These parameters were chosen to accurately assess the yield strength. The initial dimensions of the test samples were recorded and secured between the top and bottom jaws of the UTM machine. The upper jaw would ascend to increase the tension at a designated crosshead speed during the operation. The force was maintained until the elastic region of the nanocomposite was reached, allowing for the calculation of the samples' yield strength. The yield capacity of the samples was determined by analyzing the elastic area of the nanocomposite. The samples were retrieved once the yield capacity test had finished, and their ultimate elongation was measured. The percentage of elongation was calculated by determining the difference between each sample's final and original length.

Wear test

The wear rates were determined using high-precision (0.1 mg) analytical balances. The values measured with these balances had an accuracy of 0.01-0.1 mg, as reported in the pin-on-disk experiment (Ducom, Model No. TR-201 CL, Bangalore, India). The specimens for the wear test had a diameter of 8 mm and a length of 25 mm. These samples were placed on the rotating disk, and a frictional

load was applied to them. The disk used in this study was made of EN31 steel, measuring 165 mm in diameter and 8 mm in thickness [24]. After every test, the pin and disk faces were thoroughly washed using acetone. A counterweight of 10 N was applied, and the disk speed was maintained at 50 m/sec for a test period of 30 min [25].

Coefficient of linear thermal expansion

Following ASTM E228, the coefficient of linear thermal expansion (CLTE) of the samples was measured. Specimens with a length of 30 mm and a diameter of 8 mm were tested using a MIE 390 dilatometer [8]. The experiment employed a linear variable differential transformer (LVDT) with a measurement range of 5 mm as well as maximum and minimum applied temperatures of 25 and 300 °C, respectively, and a temperature ramp rate of 5 °C/min. The dilatometer was used in an experiment performed at VB Ceramics, Chennai, India. The sensing function (the variable capacitor transducer) and dial indicator were operated by a specimen on the sensor surface by means of a push pin which measures the coefficient of thermal expansion with the help of Eq. (6) [26], [27].

$$CLET\left(\bar{\alpha}\right)=\left(\frac{L_f-L_i}{L_i(T_f-T_i)}\right) \tag{6}$$

where $(\bar{\alpha})$ is the CLTE, L_f is the length at the final temperature, L_i is the length at the intial temperature, T_f is the final temperature, and T_i is the initial temperature. The thermal conductivity of the Al/ZrO_2 nanocomposite had already been investigated using laser flash analysis (LFS 457) equipment, which enabled the accurate determination of the material's thermal diffusivity and thermal conductivity. The Al/ZrO_2 nanocomposite specimens, with dimensions of 10 mm in diameter and 3 mm in thickness, were then prepared, and their surfaces were polished for uniform flatness. The experiment was conducted at a room temperature of 25 °C raising this value up to 300 °C. The thermal conductivity of each specimen was calculated using Eqs. (7) and (8) [28], [29].

$$Thermal\ conductivity(k)=\alpha.\rho.C_p \tag{7}$$

where k denotes the thermal conductivity ($Wm^{-1}K^{-1}$); α is thermal diffusivity (m^2/s), measured by LFA; ρ is the density of the specimen (kg/m^3); and C_p is the specific heat capacity (J/kg. K).

$$Thermal\ conductivity(\alpha)=\left(\frac{0.1388.L^2}{t_{1/2}}\right) \tag{8}$$

where α is the thermal diffusivity (m^2/s), L is the specimen thickness (mm), and $t_{1/2}$ is the time required for the rear face of the specimen to reach half the maximum temperature.

Result and discussion

Microstructural analysis

In AZ0, the pure aluminum sample, the image reveals a characteristic Al matrix and clear particle bonding without any reinforcement particles (Figure 4). AZ3, reinforced with 3%ZrO_2, exhibits ZrO_2 particles scattered throughout the Al, as well as a certain porosity. The ZrO_2 particles bonded well with the Al. However, some of the pores are still visible in the structure. In AZ6, which has 6% ZrO_2, the SEM image indicates ZrO_2 agglomeration. Thus, it is expected that the particles will cluster, oxide particles will form, and the resulting composite will exhibit moderate porosity [30]. This implies that an increased concentration of ZrO_2 leads to the partial clustering of the reinforcing particles, which would impact the homogeneity of the composite. Finally, AZ9, with the greatest reinforcement content (9% ZrO_2) demonstrated a pronounced agglomeration of ZrO_2 particles along with the presence of oxide particles. The higher concentration of ZrO_2 promotes particle clustering, which may adversely affect the strength and interfacial cohesion of the material [31]. The SEM images reveal microstructural features, such as particle bonding, ZrO_2 particles, and porosity, which are important in understanding the interaction between the Al matrix and the ZrO_2 reinforcement. Porosity is evidence of incomplete densification and the presence of oxide particles that may enhance the material's resistance to wear and corrosion. These microstructural characteristics play a crucial role in determining the mechanical and thermal characteristics of the nanocomposite materials; an ideal particle dispersion and low porosity would be desirable for improved performance.

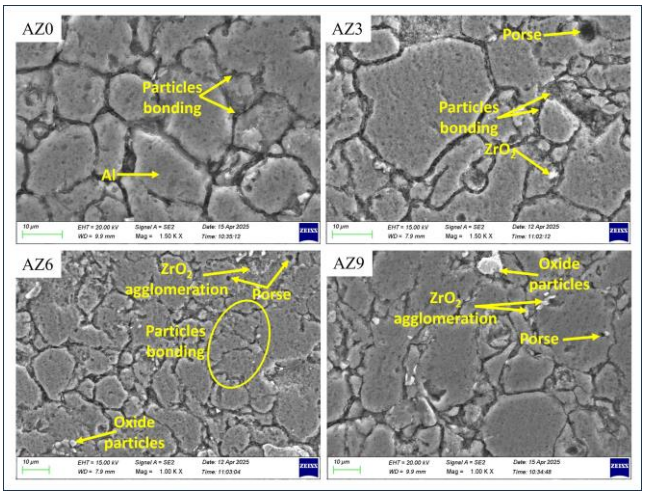

Figure 4. SEM image of Al/ZrO_2 nanocomposite samples
Source: Authors

SEM and EDX analysis

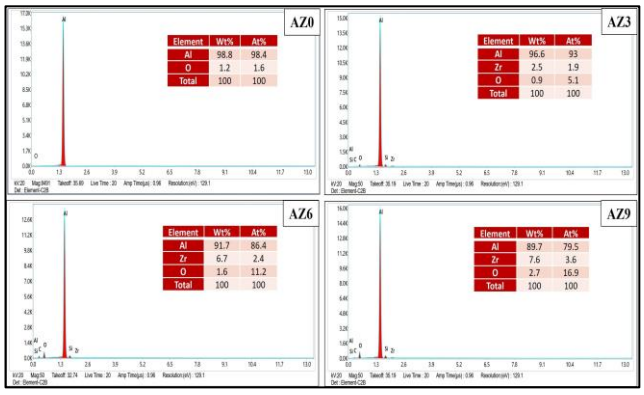

Figure 5. EDX image of Al/ZrO_2 nanocomposite samples
Source: Authors

The elemental composition of the nanocomposite samples is presented in the EDX images shown in Figure 5. The AZ0 sample contains 98.8 wt.% Al and 1.2 wt.% O, *i.e.*, it features a prevailing composition of Al (98.4 at.%). As for AZ3, the composition is 96.6 wt.% ZrO_2, 2.5 wt.% Zr, and 0.9 wt.% O [32]. The corresponding atomic percentages are 93.0 at.% Al, 1.9 at.% Zr, and 5.1 at.% O, indicating a shift as a result of adding zirconium oxide. The AZ6

sample, consists of 91.7 wt.% Al, 6.7 wt.% Zr, and 1.6 wt.% O, with atomic percentages of

86.4, 11.2, and 2.4 at.%, respectively. The introduction of Zr also increases the Zr content in the atomic percentage, meaning that ZrO_2 considerably changes the composition of the material [33]. Similarly, the AZ9 sample exhibits 89.7 wt.% Al, 7.6 wt.% Zr, and 2.7 wt.% O, with 79.5, 16.9, and 3.6 at.%. This addition of Zr further reduces the Al and increases the percentage of zirconium and oxygen in the composite [34]. The EDX spectra confirm the anticipated elemental distribution as well as the variation in the Al matrix when zirconium oxide is added. This compositional variation directly influences key material characteristics such as thermal conductivity, expansion, and the overall structural performance.

XDR analysis

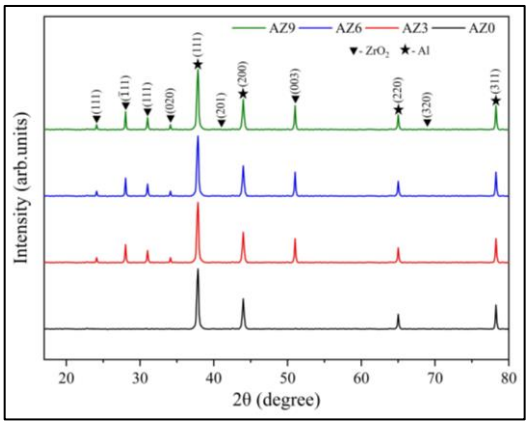

Figure 6. X-ray diffraction analysis of Al/ZrO_2 nanocomposite samples
Source: Authors

X-ray diffraction (XRD) analysis revealed the structural characteristics of the Al and Al/ZrO_2 nanocomposites, the functions of the ZrO_2 composition through phase identification, and the overall material structure. Pure Al (AZ0) exhibited X-ray peaks at 111, 200, 220, and 311 at diffraction angles of 38.47, 44.869, 65.478, and 78.236°, respectively, in accordance with JCPDS card no. 04-0787 [35], [36]. The incorporation of 3 wt.% ZrO_2 (AZ3) resulted in new peaks, confirming the presence of zirconia reinforcements. The ZrO_2 peaks intensified in AZ6 and AZ9, which demonstrates an increased ZrO_2 content in the composite material (Figure 6). The addition of more ZrO_2 causes a slight decrease in the intensity of the Al peaks due to the change in the phase distribution [37]. The analysis of diffraction patterns revealed no intermetallic compound formation in the nanocomposites, which suggests structural stability. The peak enlargement observed in the nanocomposite samples can be attributed to microstructural refinement, residual stress, and lattice strain. The XRD pattern of the ZrO_2 nanoparticles synthesized via the co-precipitation method was recorded over a 2θ range of 20-80°. The XRD pattern associated with ZrO_2 is in line with JCPDS card number 37-1484 [38]. The peak intensity increase of ZrO_2 indicates that ceramic reinforcement was successfully integrated, which can lead to enhanced mechanical properties. The existence of both Al and ZrO_2 nanoparticles demonstrates the successful formation of the Al nanocomposites. The experiment shows that ZrO_2 content can be increased to improve hardness, wear resistance, and thermal stability thanks to the properties of ceramic materials. The uniform distribution of ZrO_2 remains essential to obtain desirable mechanical, tribological, and thermal expansion.

Impact of ZrO_2 on the green density of the nanocomposites

Figure 7 illustrates the correlation between compaction pressure and green density for the Al nanocomposites. For all compositions, the green density increases steadily as the pressure is increased between 400 and 600 MPa. This trend was observed in each group. The AZ0 sample exhibits the lowest green density, reaching 1.56 g/cm³ at 400 MPa. Its maximum density is 2.36 g/cm³ at 600 MPa. The addition of ZrO_2 increases the green density, with AZ9 showing the highest values, reaching of 2.63 g/cm³ at maximum pressure. An intermediate behavior is observed for AZ3 and AZ6, whereas the green compaction density of AZ6 (2.49 g/cm³) is slightly higher than that of AZ3 over the entire pressure range. These results indicate that, the more ZrO_2 is incorporated into the Al matrix, the greater the density of the green compaction at any pressure level, highlighting the beneficial effect of ceramic reinforcement on the compact behavior of Al nanocomposites. This trend is important for understanding the material properties of Al nanocomposites in applications requiring high-density materials.

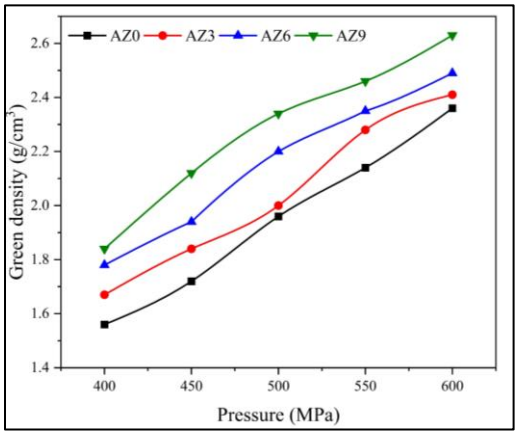

Figure 7. Green density *vs.* pressure for Al/ZrO_2 nanocomposites
Source: Authors

Density and porosity

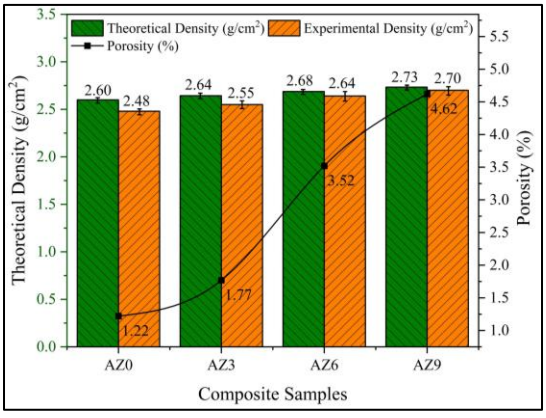

Figure 8. Density measurement of Al/ZrO_2 nanocomposite samples
Source: Authors

The porosity of sample AZ0 was 1.22%, while that of AZ3 was 1.77% at the initial stage. Sample AZ6 exhibited a peak porosity of

3.52%, indicating its potential for complete densification. The porosity was reduced to 4.62% for sample AZ9. Figure 8 shows a comparative analysis of theoretical and experimental density values for Al-matrix nanocomposites reinforced with varying concentrations of zirconia (ZrO_2) at 3, 6, and 9 wt.%. The theoretical density was calculated using the rule of mixture, while the experimental density was measured using Archimedes' principle [20]. The theoretical density increased with the increase in reinforcement nanoparticles, *i.e.*, 2.6, 2.64, 2.68, and 2.73 g/cm³, while the experimental density was slightly lower, with 2.48, 2.55, 2.64, and 2.7 g/cm³, due to the compaction pressure and sintering temperature effects. Theoretical density was calculated based on the proportional contribution of the individual constituent densities. The observed increase in density is attributed to the additions of ZrO_2, which is denser than Al [39]. Previous studies have reported that, when optimizing their processing, Al nanocomposites containing ceramic particulates exhibit improved densifications. The slight deviation between theoretical and experimental values indicates improper material packing, a phenomenon commonly reported in Al nanocomposites fabricated via powder metallurgy [40].

Density of green compaction and sintered nanocomposites

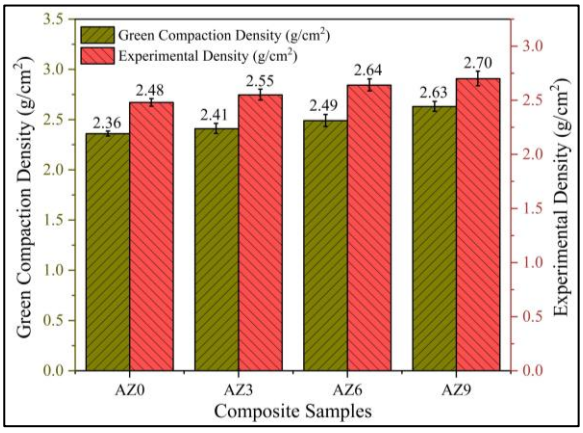

Figure 9. Comparison of green compaction and experimental densities for Al/ZrO_2 nanocomposites
Source: Authors

Figure 9 compares the green compaction density and the experimental density of four Al nanocomposite samples. The green compaction density represents the density of the samples obtained immediately after compaction process, while the experimental density corresponds to the density of the samples after the sintering process. The findings suggest that, in general, green compaction densities increase with the incorporation of ZrO_2, rising from 2.36 g/cm³ for AZ0 to 2.63 g/cm³ for AZ9. This trend reflects increased packing ability and contact of the particles with the correspondingly decreasing concentration of reinforcement material [41]. A similar trend is observed after sintering, with AZ9 exhibiting the highest density (2.7 g/cm³). The post-sintering density increase is greater with a higher content of ZrO_2 samples. The nanocomposite samples exhibit differences between green and sintered densities of 0.12, 0.14, 0.15, and 0.07 g/cm³. Thus, the sintering process becomes more effective at reducing porosity and enhancing the cohesion of the material, particularly in the samples with high reinforcement contents [42]. This also implies that the addition of ZrO_2 enhances the densification of the Al matrix, with AZ9 demonstrating the most promising outcome in terms of both green compaction and sintered density. The results indicate that ZrO_2 reinforcement has a beneficial effect on the density and overall material properties of the aluminum nanocomposites.

Hardness and compression

The experimental results demonstrate that variations in the ZrO_2 reinforcement content significantly affect both hardness and compressive strength. The hardest base (AZ0) has a compressive strength of 43 MPa and the lowest hardness (33 HV). The addition of ZrO_2 to the material (AZ3) yielded outstanding improvements in mechanical properties, with a hardness of 58 HV and a compressive strength of 290 MPa. In AZ6, the material hardness reached 74 HV, while the compressive strength reached 332 MPa. The mechanical properties of AZ9 peaked at 87 HV [43] and 376 MPa [44], respectively. The results indicate that the mechanical properties of the material improved systematically as the reinforcement content increased. Data analysis reveals that the rate of increase in compressive strength exceeded the rate of hardness expansion by a notable margin. Specifically, the compressive strength increased from 43 to 290 MPa between AZ0 and AZ3. Figure 10 shows that hardness grows at a steady rate, which is lower than the increase rate of the compressive strength. Although the incremental improvement in compressive strength observed from AZ6 to AZ9 is smaller than that from AZ3 to AZ6, AZ9 exhibits a superior overall resistance compared to AZ6. Composition plays an important role in material strengthening, as there is a direct proportionality between reinforcement content and mechanical properties. The mechanical properties of AZ9 reach their peak when the reinforcement content is maximized [45]. The test results demonstrate that reinforcement is one of the essential factors to be taken into account when enhancing hardness and compressive strength. This validates the use of the studied materials in applications requiring high wear resistance and mechanical strength.

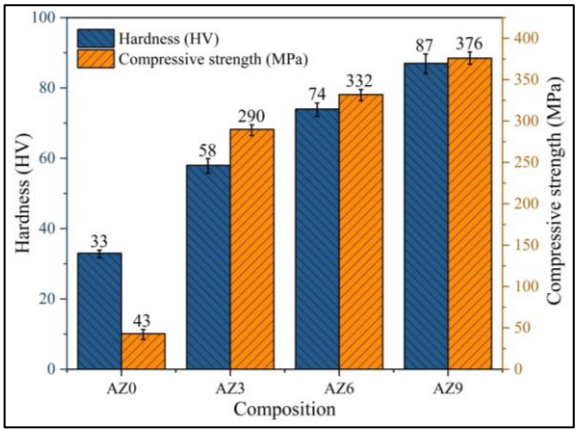

Figure 10. Hardness and compressive strength of Al/ZrO_2 nanocomposite samples
Source: Authors

Tensile and elongation test

The addition of reinforcement particles in metal matrix nanocomposites results in enhanced tensile strength and strain relationship behaviors, given their inverse relationship pattern, as shown in Figure 11. The addition of ZrO_2 enhances the resistance of the materials to tension failures. However, it simultaneously decreases ductility, leading to a reduction of the elongation values. The tensile strength in pure Al (AZ0) amounted to 180 MPa, with an elongation of 9.5%, which produced a soft and ductile material. The tensile strength reached 220 MPa in AZ3, which contained 3% ZrO_2, but the elongation level decreased to 8%, exhibiting

reduced material flexibility. The AZ6 mixture showed a tensile strength of 245 MPa, accompanied by a reduced elongation (7%) which indicates increased material brittleness. In sample AZ9, tensile strength reached its maximum value of 285 MPa [46]. However, this enhancement yielded a decrease in elongation (6%) through the brittle-strength relationship. An increase in ZrO_2 content improved the resistance of the material to deformation. However, it simultaneously induced brittleness under impact due to the associated increase in strength [47]. The wear properties of materials are improved when integrated with ZrO_2 content, as the ceramic phase provides rigid load-bearing capacity and enhances the hardness of the protective surface. Additionally, the coefficient of thermal expansion of the nanocomposites decreases with increasing ZrO_2 content, as ceramic reinforcements restrict overall matrix expansion and thereby improve dimensional stability at elevated temperatures [48]. The reinforcement particles also increase stiffness, enhancing load-bearing capability while reducing ductility and limiting formability. The ZrO_2 nanoparticles were uniformly distributed within our Al matrix, which improved fatigue resistance for load distribution [49]. Optimizing the ZrO_2 content is one of the most crucial processes for attaining the right balance between mechanical strength, wear resistance, and thermal expansion control in nanocomposites.

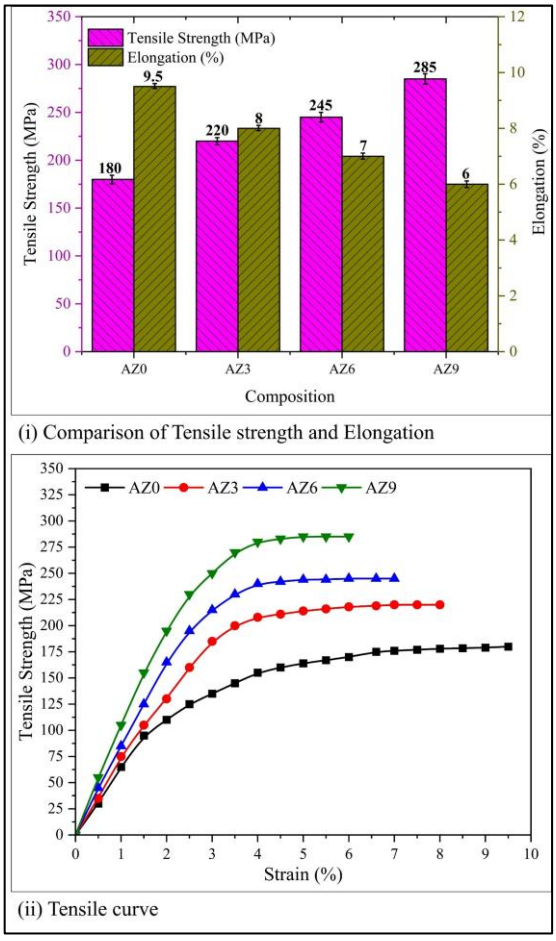

Figure 11. Tensile strength and strain relationship of Al/ZrO_2 nanocomposites
Source: Authors

Wear analysis

Figure 12 illustrates the coefficient of friction (COF) of the four samples, measured over a period of 30 min. Sample AZ0, representing pure Al, yielded the highest values of COF (between 1.4 and 1.6), with apparent variations during the testing period. This behavior is attributed to the absence of reinforcing particles, which leads to increased frictional interaction. In comparison, sample AZ3, containing 3% ZrO_2, showed a reduced COF in the range of 1.0 and 1.2, indicating that the addition of ZrO_2 effectively lowers friction relative to pure Al. Further improvements were observed in sample AZ6, which exhibited a COF of 0.8-1.0, reflecting greater stability and reduced friction [50]. This behavior can be attributed to the higher concentration of ZrO_2, which promotes the formation of an oxide coating that acts as a solid lubricant, reducing material-to-material contact. Sample AZ9 exhibited the lowest and most constant values of COF, ranging between 0.2 and 0.4 [51]. These minimal fluctuations indicate that an increased amount of ZrO_2 has a significant influence on the tribological workability of Al, substantially reducing friction. Overall, the results demonstrate a clear trend: a higher ZrO_2 content corresponds to lower COF values, which indicates better frictional behavior [52]. Owing to its enhanced wear resistance, AZ9 emerges as the most promising candidate for application in high-friction environments, such as high-performance and automobile bearings. These findings confirm the potential of aluminum-ZrO_2 nanocomposites for enhancing tribological performance.

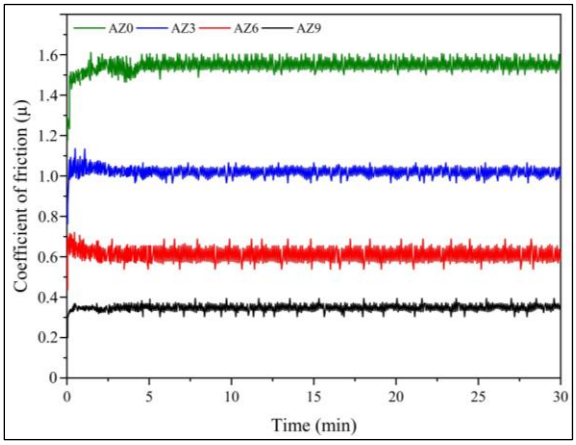

Figure 12. Wear coefficient of friction for Al/ZrO_2 nanocomposite samples
Source: Authors

Thermal conductivity and linear thermal expansion

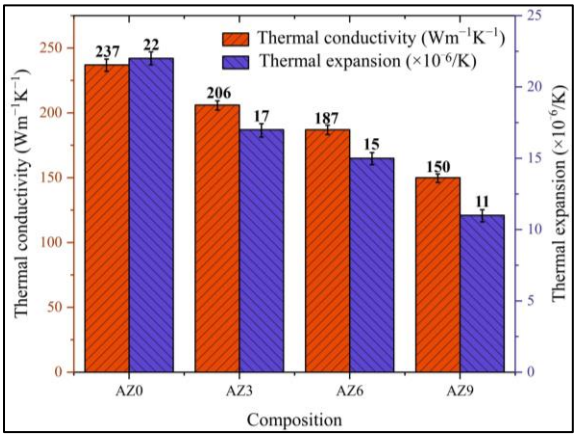

Figure 13. Thermal conductivity and linear thermal expansion of Al/ZrO_2 nanocomposite samples
Source: Authors

Figure 13 presents the thermal conductivity and thermal expansion data for various nanocomposite compositions. The incorporation of ZrO_2 into the composite material leads to a reduction in thermal conductivity. Sample AZ0 exhibited the highest thermal conductivity value of 237 $Wm^{-1}K^{-1}$, while AZ9 showed the lowest value: 150 $Wm^{-1}K^{-1}$. This reduction is also explained by the phonon scattering effect that arises when ZrO_2 is added. Heat transfer occurs through phonons, which are more likely to scatter at the interfaces between the Al matrix and the ZrO_2 phase [53]. This scattering disrupts the uniform distribution of thermal energy, thus impeding heat conduction and reducing the overall thermal conductivity of the composite. Conversely, linear thermal expansion increases with increasing ZrO_2 contents. Sample AZ0 exhibited the lowest thermal expansion (22 $\times 10^{-6}$/K) and AZ9 the highest (11 $\times 10^{-6}$/K) [54], [55]. This increase can be attributed to the difference in the thermal expansion rate of Al and the ZrO_2 ceramic phase, which induces volumetric changes upon heating. It is also associated with the difference in the CTE of the Al matrix and the ceramic reinforcement [56], [57]. These differences generate internal stresses and dimensional changes during thermal cycling. Due to the combined effects of reduced thermal conductivity caused by phonon scattering and high thermal expansion resulting from CTE mismatch, these composites are suitable for applications requiring controlled thermal management. This is a trade-off between thermal conductivity and expansion that should be carefully considered during material design.

Conclusion

This study focused on analyzing the behavior of aluminum matrix nanocomposites reinforced with ZrO_2 nanoparticles fabricated via the powder metallurgy technique. Al/ZrO_2 nanocomposites were produced with varying reinforcement contents of 3, 6, and 9 wt.%. The microstructure, mechanical properties, wear coefficient of friction, and thermal expansion of pure aluminum and Al/ZrO_2 nanocomposites were systematically evaluated. The conclusions of our work are presented below:

- The AZ9 nanocomposite sample, containing 9 wt.% of ZrO_2 nanoparticles, achieved the highest density (2.70 g/cm³) and a porosity of 4.62%. This enhancement resulted from optimized compaction pressure and a controlled sintering process.
- The microhardness and compressive strength of the nanocomposite increased progressively from sample AZ0 to sample AZ9. The increased ZrO_2 nano-reinforcement also resisted particle dislocation and fine densification. Higher compaction pressure during the fabrication further improved particle bonding and minimized internal defects. The AZ9 nanocomposites achieved a microhardness of 87 HV and a compressive strength of 376 MPa, significantly outperforming the unreinforced AZ0 sample.
- The addition of ZrO_2 nano-reinforcement significantly improved the wear resistance of the Al nanocomposites. Although ceramic reinforcement reduced the ductility of Al, it enhanced hardness, toughness, and heat resistance in friction to resist the wear. Consequently, the AZ9 nanocomposite exhibited low friction during sliding, resulting a decrease in the coefficient of friction: from 0.45 µm in the unreinforced AZ0 sample to 0.31 µm in the AZ9 sample.
- The outcome of thermal stability of Al/ZrO_2 nanocomposite improved with increasing ZrO_2 reinforcement content. Both the thermal conductivity and linear thermal expansion were steadily reduced due to the ceramic nature of ZrO_2, which acts as a thermal barrier within the Al matrix. The presence of the reinforcement nanoparticles effectively precluded the heat flow and resisted dimensional changes at elevated temperatures. Among all samples, the AZ9 nanocomposite demonstrated the lowest thermal conductivity (150 $Wm^{-1}K^{-1}$), as well as a low thermal expansion value (11×10^{-6}/K).

Acknowledgements

The authors express their sincere gratitude to Saveetha Institute of Medical and Technical Sciences (SIMATS) for its continuous academic and institutional support throughout this research.

CRediT author statement

Author 1: Conceptualization, data curation, formal analysis, writing (review and editing)
Author 2: methodology, investigation, supervision, validation

Access to research data

The datasets produced and examined in this investigation can be obtained from the authors upon reasonable request.

Conflicts of interest

The authors declare that there are no conflicts of interest concerning this research.

Statement on artificial intelligence

The authors utilized ChatGPT to improve grammar and clarity in specific sections of the document. All generated content was reviewed and revised by the authors, who assume full responsibility for the material presented in this publication.

References

[1] Á. Tóth, Á. I. Szabó, and R. Kuti, "Tribological properties of nano-sized ZrO_2 ceramic particles in automotive lubricants," *FME Trans.*, vol. 49, no. 1, pp. 36–43, 2021. https://doi.org/10.5937/fme2101036t

[2] P. P. Fedorov and E. G. Yarotskaya, "Zirconium dioxide. Review," *Condens. Matter Interphases*, vol. 23, no. 2, pp. 169–187, Jun. 2021. https://doi.org/10.1730/kcmf.2021.23/3427

[3] E.-S. R. Khattab, S. S. Abd El Rehim, W. M. I. Hassan, and T. S. El-Shazly, "Band structure engineering and optical properties of pristine and doped monoclinic zirconia (m-ZrO_2): Density functional theory theoretical prospective," *ACS Omega*, vol. 6, no. 44, pp. 30061–30068, 2021. https://doi.org/10.1021/acsomega.1c04756

[4] X. Song *et al.*, "Thermophysical and mechanical properties of cubic, tetragonal and monoclinic ZrO_2," *J. Mater. Res. Technol.*, vol. 23, pp. 648–655, 2023. https://doi.org/10.1016/j.jmrt.2023.01.040

[5] M. Petriceanu *et al.*, "Effect of doping ZrO_2 on structural and thermal properties," *Inorganics*, vol. 12, no. 11, art. 290, 2024. https://doi.org/10.3390/inorganics12110290

[6] J. Kumar *et al.*, "Investigation on the mechanical, tribological, morphological and machinability behavior of stir-casted Al/SiC/Mo reinforced MMCs," *J. Mater. Res. Technol.*, vol. 12, pp. 930–946, 2021. https://doi.org/10.1016/j.jmrt.2021.03.034

[7] F. Rocha and S. Simões, "Aluminum nanocomposites reinforced with Al_2O_3 nanoparticles: Synthesis, structure, and properties," *J. Compos. Sci.*, vol. 8, no. 1, art. 33, 2024. https://doi.org/10.3390/jcs8010033

[8] B. Anjaneyulu, G. Nagamalleswara Rao, and K. Prahlada Rao, "Development, mechanical and tribological characterization of Al_2O_3 reinforced ZrO_2 ceramic composites," *Mater. Tod. Proc.*, vol. 37, pp. 584–591, 2021. https://doi.org/10.1016/j.matpr.2020.05.594

[9] M. Pul, "Effect of ZrO_2 quantity on mechanical properties of ZrO_2-reinforced aluminum composites produced by the vacuum infiltration technique," *Rev. Metal.*, vol. 57, no. 2, pp. 1-13, 2021. https://doi.org/10.3989/revmetalm.195

[10] K. Sabari, A. Muniappan, B. Deepanraj, and M. Yuvaperiyasamy, "Exploring the effect of TiO_2 nanoparticles on the microstructural dynamics and mechanical attributes of dissimilar FSW joints between AA7071 and AZ31," *Trans. Indian Inst. Met.*, vol. 78, no. 3, art. 66, 2025. https://doi.org/10.1007/s12666-024-03535-1

[11] S. Rajaram, P. Karthikeyan, T. Jaya Surya, K. Kaniskar, and V. Pazhanivel, "Experimental investigation of mechanical properties of AA6063/ZrO_2 metal matrix composites," *Mater. Today Proc.*, vol. 74, pp. 105–109, 2023. https://doi.org/10.1016/j.matpr.2022.12.129

[12] M. Kalaimani and S. Tajudeen, "Investigation of wear performance in zirconium dioxide reinforced aluminum hybrid nanocomposites synthesized by the powder metallurgy process," in *SAE Technical Paper Series*, no. 2023-01-5161, 2024, https://doi.org/10.4271/2023-01-5161

[13] P. Haja Syeddu Masooth, G. Bharathiraja, V. Jayakumar, and K. Palani, "Microstructure and mechanical characterisation of ZrO_2 reinforced Ti6Al4V metal matrix composites by powder metallurgy method," *Mater. Res. Express*, vol. 9, no. 2, art. 020003, 2022. https://doi.org/10.1088/2053-1591/ac5352

[14] K. Sabari, A. Muniappan, B. Deepanraj, and M. J. S. Mohamed, "Enhancing mechanical performance of friction stir welded AZ31 magnesium alloy with nano-TiC reinforcements using Grey relational analysis," *Int. J. Precis. Eng. Manuf.*, vol. 26, no. 1, pp. 27–41, 2024. https://doi.org/10.1007/s12541-024-01096-3

[15] S. Kaliappan, M. Appusamy, and M. Singh, "Mechanical characterization of friction stir welded magnesium alloy reinforced with titanium carbide nanofibers," *Sold. Inspeç.*, vol. 29, art. e014, 2024. https://doi.org/10.1590/0104-9224/si29.14

[16] K. M and S. Tajudeen, "Investigation of the microstructure and mechanical properties of an Al/SiC/ZrO_2 hybrid composite by spark plasma sintering technique," *Gazi Univ. J. Sci.*, vol. 37, no. 3, pp. 1461–1478, 2024. https://doi.org/10.35378/gujs.1348461

[17] A. M. Sankhla *et al.*, "Effect of mixing method and particle size on hardness and compressive strength of aluminum-based metal matrix composite prepared through powder metallurgy route," *Mater. Res. Technol.*, vol. 18, pp. 282–292, 2022. https://doi.org/10.1016/j.jmrt.2022.02.094

[18] G. B. V. Kumar, R. Pramod, C. G. Sekhar, G. P. Kumar, and T. Bhanumurthy, "Investigation of physical, mechanical and tribological properties of Al6061–ZrO_2 nano-composites," *Heliyon*, vol. 5, no. 11, art. e02858, 2019. https://doi.org/10.1016/j.heliyon.2019.e02858

[19] D. S. Prasad, C. Shoba, and N. Ramanaiah, "Investigations on mechanical properties of aluminum hybrid composites," *J. Mater. Res. Technol.*, vol. 3, no. 1, pp. 79–85, 2014. https://doi.org/10.1016/j.jmrt.2013.11.002

[20] T. Shaafi, M. Kalaimani, S. Karthick, and N. Senthilkumar, "Effect of SiC and B_4C reinforcements on the structural and mechanical properties of aluminum composites fabricated by spark plasma sintering," *Evergreen*, vol. 12, no. 2, pp. 1322–1335, 2025. https://doi.org/10.5109/7363512

[21] P. Bharathi and T. S. Kumar, "Mechanical characteristics and wear behaviour of Al/SiC and Al/SiC/B_4C hybrid metal matrix composites fabricated through powder metallurgy route," *Silicon*, vol. 15, no. 10, pp. 4259–4275, 2023. https://doi.org/10.1007/s12633-023-02347-0

[22] A. Comba *et al.*, "Vickers hardness and shrinkage stress evaluation of low and high viscosity bulk-fill resin composite," *Polymers.*, vol. 12, no. 7, art. 1477, 2020. https://doi.org/10.3390/polym12071477

[23] A. Asmare, R. Al-Sabur, and E. Messele, "Experimental investigation of friction stir welding on 6061-T6 aluminum alloy using Taguchi-based GRA," *Metals.*, vol. 10, no. 11, art. 1480, 2020. https://doi.org/10.3390/met10111480

[24] N. Senthilkumar, B. Deepanraj, F. Shaik, and V. Nadanakumar, "Wear studies on nano silicon carbide particle strengthened AZ31 magnesium nano surface composites developed via friction stir processing," *Turk. J. Eng.*, vol. 9, no. 3, pp. 425–432, 2025. https://doi.org/10.31127/tuje.1531603

[25] S. Dhanalakshmi, K. ShanmugaSundaram, T. Tamilarasan, and R. Rajendran, "The role of ceramic particle loading and the influence of hot extrusion on the tribological behaviour of aluminium alloy-SiCp composites," *J. Compos. Mater.*, vol. 55, no. 5, pp. 687–701, Sep. 2020. https://doi.org/10.1177/0021998320957405

[26] K. Kang, S.-M. Hong, C. Lee, and Y. Cho, "Thermal expansion of ZrO_2-20 mol% Gd_2O_3," *Arch. Metall.*, vol. 66, no. 4, pp. 909–912, Nov. 2021. https://doi.org/10.24425/amm.2022.139682

[27] J. Huang, C. Yang, Q. Huang, Z. Deng, Y. Wang, X. Li, Z. Zhou, J. Chen, Z. Liu, and W. Guo, "Optical, thermal, and mechanical properties of (y1-xscx)2o3 transparent ceramics," *J. Adv. Ceram.* vol. 11, no. 6, pp. 1–22, 2021. https://doi.org/10.21203/rs.3.rs-1113962/v1

[28] T. Huber, H. P. Degischer, G. Lefranc, and T. Schmitt, "Thermal expansion studies on aluminium-matrix composites with different reinforcement architecture of SiC particles," *Comp. Sci. Technol.*, vol. 66, no. 13, pp. 2206–2217, 2006. https://doi.org/10.1016/j.compscitech.2005.12.012

[29] T. Shaafi, M. Kalaimani, M. Yuvaperiyasamy, V. Jeyabalaji, and Krishna Prakash Arunachalam, "Microstructural, mechanical, and thermal characterization of TiO_2- and ZrO_2-reinforced aluminum matrix nanocomposites fabricated using powder metallurgy," *J. Environ. Nanotechnol.*, vol. 14, no. 2, pp. 253–264, 2025. https://doi.org/10.13074/jent.2025.06.2521466

[30] N. Kumar and I. G., "A review on tribological behaviour and mechanical properties of Al/ZrO_2 metal matrix nano composites," *Mater. Today Proc*, vol. 38, pp. 2649–2657, 2021. https://doi.org/10.1016/j.matpr.2020.08.240

[31] H. Zhu *et al.*, "Microstructure and high temperature wear of the aluminum matrix composites fabricated by reaction from Al–ZrO2–B elemental powders," *Powder Technol.*, vol. 217, pp. 401–408, 2012. https://doi.org/10.1016/j.powtec.2011.10.056

[32] M. Yadav, L. A. Kumaraswamidhas, and S. K. Singh, "Investigation of solid particle erosion behavior of Al-Al2O3 and Al-ZrO_2 metal matrix composites fabricated through powder metallurgy technique," *Tribol. Int.*, vol. 172, art. 107636, 2022. https://doi.org/10.1016/j.triboint.2022.107636

[33] I. Rosales-Cadena *et al.*, "The effect of ZrO_2 addition and thermal treatment on the microstructure and mechanical properties of aluminum metal matrix composites (AMMCs)," *Materials*, vol. 18, no. 19, art. 4507, Sep. 2025, https://doi.org/10.3390/ma18194507

[34] W. S. AbuShanab, E. B. Moustafa, E. Ghandourah, and M. Taha, "A comprehensive study of Al–Cu–Mg system reinforced with nano-ZrO_2 particles synthesized by powder metallurgy technique," Research Square, preprint, Mar. 2021. [Online]. Available: https://doi.org/10.21203/rs.3.rs-326782/v1

[35] K. Pal, K. Navin, and R. Kurchania, "Study of structural and mechanical behaviour of Al-ZrO_2 metal matrix nanocomposites prepared by powder metallurgy method," *Mater. Today Proc.*, vol. 26, pp. 2714–2719, 2020. https://doi.org/10.1016/j.matpr.2020.02.570

[36] P. R. Rauta, P. Manivasakan, V. Rajendran, B. B. Sahu, B. K. Panda, and P. Mohapatra, "Phase transformation of ZrO_2 nanoparticles produced from zircon," *Phase Trans.*, vol. 85, no. 1–2, pp. 13–26, 2012. https://doi.org/10.1080/01411594.2011.619698

[37] P. Khajuria, R. Mahajan, and R. Prakash, "Synthesis and luminescent properties of ZrO_2 and Dy3+-activated ZrO_2 powders," *J. Mater. Sci. Mater. Electron.*, vol. 32, no. 23, pp. 27441–27448, 2021. https://doi.org/10.1007/s10854-021-07120-w

[38] O. Mangla and S. Roy, "Monoclinic zirconium oxide nanostructures having tunable band gap synthesized under extremely non-equilibrium plasma conditions," *IOCN*, 2018, p. 10, 2018. https://doi.org/10.3390/iocn_2018-1-05486

[39] J. Zhang, L. Zhang, and H. Ma, "Effect of ZrO_2 additions on the microstructure, mechanical and wear properties of ZrO_2/7075 aluminium alloy composite," *Mater. Today Commun.*, vol. 37, art. 107437, 2023. https://doi.org/10.1016/j.mtcomm.2023.107437

[40] P. Wei *et al.*, "Enhancing strength and ductility of graphene and ZrO_2 nanoparticles hybrid reinforced AA2024 composite fabricate by laser powder bed fusion," *Compos. A*, vol. 185, art. 108378, 2024. https://doi.org/10.1016/j.compositesa.2024.108378

[41] Ankur, A. Bharti, D. Prasad, N. Kumar, and K. K. Saxena, "A re-investigation: Effect of various parameter on mechanical properties of copper matrix composite fabricated by powder metallurgy," *Mater. Today Proc.*, vol. 45, pp. 4595–4600, 2021. https://doi.org/10.1016/j.matpr.2021.01.009

[42] N. Kumar, A. Bharti, D. Prasad, M. Verma, and A. Kumar Chauhan, "Investigations on physical and mechanical properties of Mg composites and foams fabricated by powder metallurgy using NaCl," *Mater. Today Proc.*, vol. 78, pp. 7–11, 2023. https://doi.org/10.1016/j.matpr.2022.09.374

[43] M. Avadi Ammal, J. Sudha, R. Vaishnavi, and S. H. Vaishnavi, "Effect of aging treatment on friction stir processed Al-ZrO_2-graphene nanoplatelet surface composite," *J. Mater. Eng. Perform*, vol. 33, no. 24, pp. 14071–14084, 2023. https://doi.org/10.1007/s11665-023-08993-0

[44] S. V. Prasat, A. Rajkumar, N. Venkateshwaran, and S. Sekar, "Microstructural characterization and investigation on mechanical properties of stir cast hybrid A356/B_4C/ZrO_2 composites with strontium as grain modifier," in *Advances in Additive Manufacturing Technologies*, G. Gurusamy, Ed., London, UK: CRC Press, 2024, pp. 129–134, 2024. https://doi.org/10.1201/9781003545774-23

[45] I. S. Patil, A. Anarghya, S. S. Rao, M. A. Herbert, and R. Kushwaha, "Effect of zirconium oxide particulate composites with Al-Si on the microstructural and mechanical properties of hot pressed, spray forming and stir casting methods," *Aust. J. Mech. Eng.*, vol. 21, no. 3, pp. 756–774, 2021. https://doi.org/10.1080/14484846.2021.1913872

[46] G. Karthikeyan, G. Elatharasan, S. Thulasi, and P. Vijayalakshmi, "Tensile, compressive and heat transfer analysis of ZrO_2 reinforced aluminum LM6 alloy metal matrix composites," *Mater. Today Proc.*, vol. 37, pp. 303–309, 2021. https://doi.org/10.1016/j.matpr.2020.05.270

[47] P. Vignesh, S. V. Alagarsamy, P. Raveendran, H. Saravanan, and K. Karthikeyan, "Effect of zirconia content on properties of Al7050 alloy composites by stir casting method," *Mater. Today Proc.*, vol. 47, pp. 4121–4125, 2021. https://doi.org/10.1016/j.matpr.2021.07.223

[48] A. V. Aborkin *et al.*, "Thermal expansion of aluminum matrix composites reinforced by carbon nanotubes with in-situ and ex-situ designed interfaces ceramics layers," *J. Alloys Compd.*, vol. 872, art. 159593, 2021. https://doi.org/10.1016/j.jallcom.2021.159593

[49] S. Aktaş and E. Anıl Diler, "Effect of ZrO_2 Nanoparticles and Mechanical milling on microstructure and mechanical properties of Al–ZrO_2 Nanocomposites," *J. Eng. Mater. Technol.*, vol. 143, no. 4 art. 041006, 2021. https://doi.org/10.1115/1.4050726

[50] T. Shaafi, M. Kalaimani, M. Yuvaperiyasamy, Krishna Prakash Arunachalam, and M. Karthigairajan, "Tribological optimization of Al/ZrO_2 nanocomposites: Influence of reinforcement content on wear performance using Taguchi method," *J. Environ. Nanotechnol.*, vol. 14, no. 2, pp. 162–177, Jul. 2025. https://doi.org/10.13074/jent.2025.06.2511453

[51] P. S. Shreyas, B. P. Mahesh, S. Rajanna, and N. Rajesh, "Evaluating the tribological properties of aluminum-based hybrid composites reinforced with Al_2O_3 amp; ZrO_2 nano particles," *Mater. Today Proc.*, vol. 45, pp. 429–433, 2021. https://doi.org/10.1016/j.matpr.2020.12.1012

[52] M. Umar, R. Muraliraja, P. Rathnakumar, and T. R. Tamilarasan, "The influence of ZrO_2 on tribological and mechanical characteristics of Al composite," *Mater. Today Proc*, vol. 115, pp. 17–23, 2024. https://doi.org/10.1016/j.matpr.2023.06.340

[53] X. Lin, Q. Xu, T. Deng, B. Yang, and L. Chen, "Improving thermal conductivity of Al/SiC composites by post-oxidization of reaction-bonded silicon carbide preforms," *Sci. Rep.*, vol. 14, no. 1, Jul. 2024. https://doi.org/10.1038/s41598-024-67653-y

[54] Y. Mi, Y. Xu, Y. Li, S. Sang, and Q. Wang, "Fabrication and thermal shock behavior of ZrO2 toughened magnesia aggregates," *Ceram. Int.*, vol. 47, no. 18, pp. 26475–26483, Sep. 2021. https://doi.org/10.1016/j.ceramint.2021.06.060

[55] H. Liu *et al.*, "Adjustable thermal expansion properties in Zr_2MoP_2O12/ZrO_2 ceramic composites," *Front. Chem.*, vol. 6, art. 347, Aug. 2018. https://doi.org/10.3389/fchem.2018.00347

[56] M. Zhao, X. Ren, and W. Pan, "Low thermal conductivity of SnO_2 - doped Y_2O_3 - stabilized ZrO_2: Effect of the lattice tetragonal distortion," *J. Am. Ceram. Soc.*, vol. 98, no. 1, pp. 229–235, 2014. https://doi.org/10.1111/jace.13313

[57] H. Liu, Z. Zhang, X. Cheng, and J. Yang, "Thermal expansion of ZrO_2–ZrW_2O_8 composites," *Int. J. Mod. Phys. B*, vol. 23, no. 06-07, pp. 1449–1454, 2009. https://doi.org/10.1142/s0217979209061081